Physics of Plasmas

BRIEF REPORT | FEBRUARY 15 2019

Temporal multiparticle Monte Carlo simulation of dual frequency single surface multipactor FREE

Asif Iqbal ; John Verboncoeur ; Peng Zhang

Check for updates

Phys. Plasmas 26, 024503 (2019)
https://doi.org/10.1063/1.5084143

View Online Export Citation

Articles You May Be Interested In

Multipactor susceptibility on a dielectric with a bias dc electric field and a background gas
Phys. Plasmas (May 2011)

Multipactor discharge in a dielectric-loaded accelerating structure
Phys. Plasmas (January 2007)

Multipactor susceptibility on a dielectric with two carrier frequencies
Phys. Plasmas (March 2018)

29 October 2024 17:02:22

AIP Publishing

AIP Publishing
Physics of Plasmas
Special Topics Open for Submissions
Learn More

Physics of Plasmas BRIEF COMMUNICATIONS scitation.org/journal/php

Temporal multiparticle Monte Carlo simulation of dual frequency single surface multipactor

Cite as: Phys. Plasmas **26**, 024503 (2019); doi: 10.1063/1.5084143
Submitted: 4 December 2018 · Accepted: 28 January 2019 ·
Published Online: 15 February 2019

View Online Export Citation CrossMark

Asif Iqbal,[1] John Verboncoeur,[1,2] and Peng Zhang[1,a)]

AFFILIATIONS

[1]Department of Electrical and Computer Engineering, Michigan State University, East Lansing, Michigan 48824-1226, USA
[2]Department of Computational Mathematics, Science and Engineering, Michigan State University, East Lansing, Michigan 48824, USA

[a)]Author to whom correspondence should be addressed: pz@egr.msu.edu

ABSTRACT

This work presents a multiparticle Monte Carlo simulation model in one dimension with adaptive time steps to investigate the time dependent physics of the single dielectric surface multipactor. Using this model, we study multipactor discharge on a dielectric with two carrier frequencies. We find that the saturation level and the oscillation pattern of the normal surface field with a parallel rf field of two carrier frequencies are different from those of single carrier frequency. Closed Lissajous curves are obtained to describe the temporal relationship between the fields normal and parallel to the surface in the ac saturation state.

Published under license by AIP Publishing. https://doi.org/10.1063/1.5084143

29 October 2024 17:02:22

Multipactor is a nonlinear phenomenon in which an electron avalanche driven by a high frequency rf field sustains itself by an exponential charge growth through secondary electron emission from a metallic or dielectric surface.[1–7] Avoiding multipactor has been a major challenge for high power microwave (HPM) sources, rf accelerators,[8] and space-based communication systems.[9,10]

The objective of this letter is twofold. First, we present a new one-dimensional multiparticle Monte Carlo (MC) simulation model with adaptive time steps as a tool to investigate the time dependent physics of a single surface multipactor discharge. Previous MC models either employed a single particle approach,[3–5] where the charge in a single weighted macroparticle is varied over time, or a variable number of particles approach,[11] where the number of particles is varied, while the charge per particle is kept fixed. The first approach offers a simple implementation, while the latter allows for better statistics in a growing discharge, but is computationally costly,[11] as the fixed time steps have to be set small compared to the time of flight of the particles between subsequent bounces on the surface.

In our model, we consider a system with many macroparticles. The number of macroparticles is held fixed throughout the simulation. Upon the impact of each macroparticle onto the surface, the charge and mass in that macroparticle and the normal electric field to the dielectric surface are updated according to the secondary electron yield (SEY)[12] and Gauss's law, respectively. This approach captures the statistics better than the single particle approach. However, since the number of macroparticles is fixed in this model, it still offers a simpler and less costly implementation than the variable number of particles approach. More importantly, the time intervals between subsequent bounces of different macroparticles on the surface are calculated *exactly*.

The second objective of this work is to implement this model and investigate the time dependent physics of the single surface multipactor with two carrier frequencies of the rf electric field. This investigation is particularly important as previous works[7] have shown that adding a second carrier mode of the rf field significantly changes the multipactor susceptibility on a single dielectric surface. A study of the time-dependent physics can offer better understanding of the multipactor dynamics.

A single dielectric surface is exposed to a parallel rf electric field, E_{rf}. An initial electric field E_{x0} is assigned normal to the dielectric surface. This initial normal electric field is very small compared to the rf amplitude ($E_{x0} \sim E_{rf0}/30$). From Gauss's law, we have $E_{x0} = \frac{\sigma_e}{2\epsilon_0}$, where $\sigma_e = \frac{N_{s0}e}{A}$ is the surface charge density, N_{s0} is the initial number of positive surface charges producing this normal electric field, and A is the surface area ($1\,m^2$). Therefore, we can calculate $N_{s0} = \frac{2AE_{x0}\epsilon_0}{e}$ from E_{x0}. A number of

Published under license by AIP Publishing

macroparticles (N = 200) are ejected from the dielectric surface at time, $t = 0$ (Fig. 1). Each macroparticle is assigned a random emission energy E_0 and random emission angle ϕ according to the following distributions:[4]

$$f(E_0) = \frac{E_0}{E_{0m}^2} e^{-\left(\frac{E_0}{E_{0m}}\right)}, \quad (1)$$

$$g(\phi) = \frac{1}{2}\sin\phi, \quad (2)$$

where E_{0m} is the peak of the distribution of emission energies. For charge neutrality, the total number of electrons in these macroparticles in flight is equal to N_{s0}. These initial electrons

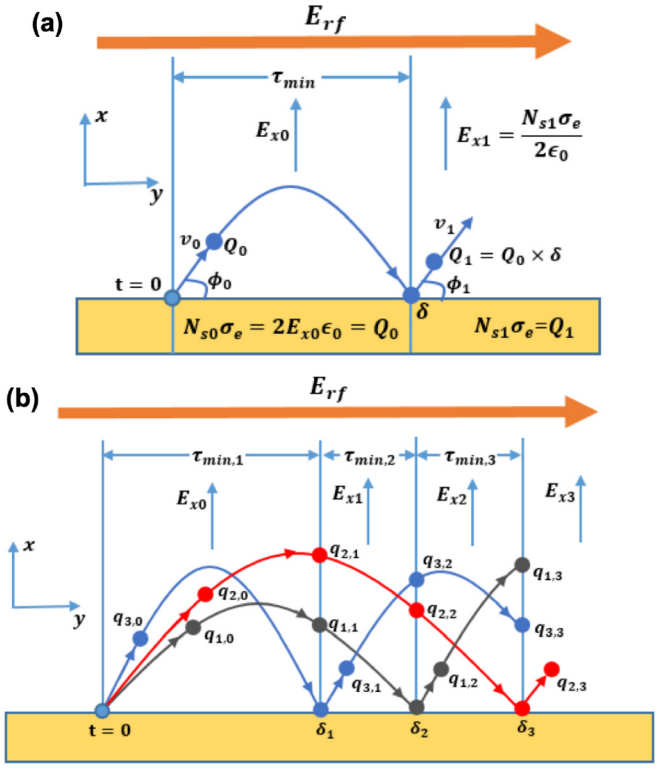

	Particle #1	Particle #2	Particle #3
Iteration #1	$q_{1,0}$	$q_{2,0}$	$q_{3,0}$
Iteration #2	$q_{1,1}=q_{1,0}$	$q_{2,1} = q_{2,0}$	$q_{3,1} = \delta_1 q_{3,0}$
Iteration #3	$q_{1,2} = \delta_2 q_{1,1}$	$q_{2,2} = q_{2,1}$	$q_{3,2} = q_{3,1}$
Iteration #4	$q_{1,3} = q_{1,2}$	$q_{2,3} = \delta_3 q_{2,2}$	$q_{3,3} = q_{3,2}$

FIG. 1. Schematic of MC modeling of the single surface multipactor discharge: (a) single particle model; the number of electrons in flight, $\mathbf{Q_i}$, total surface charge, $\mathbf{N_{si}}$, and normal electric field, $\mathbf{E_{xi}}$, are updated at each impact of a single macroparticle onto the surface, (b) Multiparticle model; multiple macroparticles are in flight, and each iteration traces one impact of a macroparticle onto the surface; the charge, $\mathbf{q_i}$, and mass, $\mathbf{m_i}$, of only the incident macroparticle hitting on the surface are updated after each iteration. Total surface charge, $\mathbf{N_{si}}$, and the normal electric field, $\mathbf{E_{xi}}$, are calculated as described in the text.

are considered to be uniformly distributed in the macroparticles. Therefore, the initial charge in jth macroparticles is $q_{j,0} = eN_{s0}/N$, where e is the electronic charge. The trajectories of the macroparticles are governed by the force law,

$$m\frac{\partial \vec{v}}{\partial t} = -|e|\left[\vec{E}_{rf} + \vec{E}_x\right]. \quad (3)$$

The macroparticles gain energy from the electric fields while in flight. After the period of flight, a macroparticle strikes the surface to eject secondary electrons.[12,13] In each iteration, we record one impact of a macroparticle upon the dielectric surface, with the transit time being calculated exactly (Fig. 1).

During the ith iteration, we first calculate the transit time, τ_j, of each macroparticle from the force law. The particle with the minimum transit time, $\tau_{min,i}$, strikes the surface first, yielding secondary electrons. We use Vaughn's empirical formula[12,13] to calculate the secondary electron yield (SEY), δ, at each impact.

If the kth macroparticle with charge $q_{k,(i-1)}$ strikes the surface at the ith impact and the secondary electron yield for this impact is δ_i, then the charge in the kth macroparticle is updated for the next iteration as $q_{k,i} = \delta_i q_{k,(i-1)}$. During this impact, $q_{k,(i-1)}$ negative charge strikes the surface and $\delta_i q_{k,(i-1)}$ negative charge is emitted from the surface. Therefore, the positive surface charge is updated for the next iteration as $N_{si} = N_{s(i-1)} + q_{k,(i-1)}(\delta_i - 1)$. The normal electric field is updated as $E_{xi} = \frac{N_{si}e}{2A\epsilon_0}$. The charge in all other macroparticles in flight remains unchanged by this impact, i.e., for any jth particle that does not strike the surface, the charge is updated as $q_{j,i} = q_{j,(i-1)}$ for the next iteration. We record the position, $x_{j,i}$, and the instantaneous velocity, $v_{j,i}$, of these macroparticles at each impact. These values are used as initial conditions to calculate transit times during the next iteration. The rf phase, θ, is updated self consistently[7] at each iteration.

The kth macroparticle, incident during the ith iteration, is then emitted from the surface again at the $(i+1)$th iteration with updated charge $q_{k,i}$, a new emission energy, E_0, and a new emission angle, ϕ, according to the distributions given by Eqs. (1) and (2). We continue this process for n impacts (or iterations). The temporal profiles of the surface charge N_s and the normal electric field to the dielectric surface E_x are obtained by converting the iteration number n into the scale of time using the transit times $\tau_{min,i}$ for each iteration.

In our MC model, the possible change of E_x during an iteration is not accounted for. The diagnostics are sampled over each iteration time step. In addition, space charge effects[14] are not considered.

The time-dependent behaviors of multipactor on a dielectric surface due to a single frequency electric field are shown in Fig. 2. In Fig. 2(a), the instantaneous parallel rf electric field, E_{rf}, and the normal electric field to the dielectric surface, E_x, are shown as functions of time. Figure 2(b) shows the corresponding secondary electron yield, δ, which oscillates at twice the rf frequency[11] in saturation and the average SEY is $\delta_{avg} = 1$. To understand the temporal relationship between the instantaneous fields acting normal and parallel to the surface, we need a susceptibility diagram obtained by applying constant electric field, $E_{y,dc}$, parallel to the surface.[11] In Fig. 2(c), this susceptibility

29 October 2024 17:02:22

Published under license by AIP Publishing

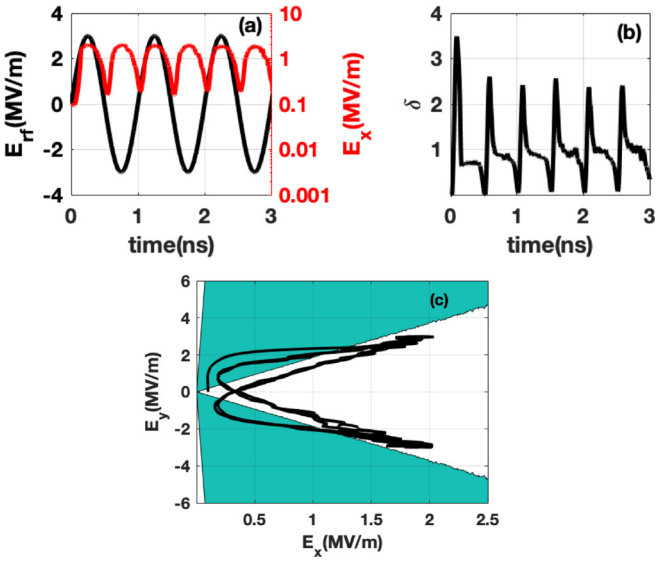

FIG. 2. Single surface multipactor with single frequency of the rf field $E_{rf} = E_{rf0}\sin(\omega t + \theta)$: (a) instantaneous total rf electric field, E_{rf}, and normal electric field, E_x, (b) secondary electron yield, δ, with the average δ_{avg}=1 for saturation, and (c) the trajectory of the electric field (E_x, E_{rf}) along with susceptibility diagram for $E_{rf0} = 3\,\mathrm{MV/m}$, $f_{rf} = 1\,\mathrm{GHz}$, and $\theta = 0$. (The blue region is susceptible to multipactor.)

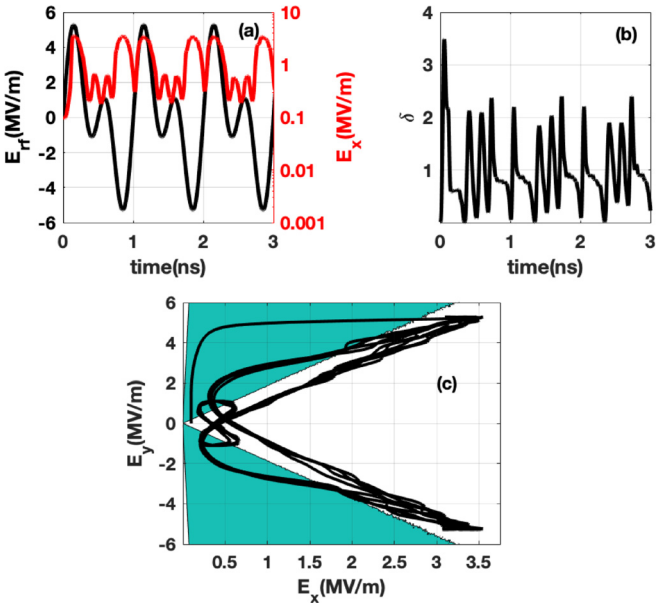

FIG. 3. Single surface multipactor with two frequencies of the rf field: (a) instantaneous total rf electric field, E_{rf}, and normal electric field, E_x, (b) secondary electron yield, δ, with the average δ_{avg}=1 for saturation, and (c) the trajectory of the electric field (E_x, E_{rf}) along with susceptibility diagram for $E_{rf0} = 3\,\mathrm{MV/m}$, $f_{rf} = 1\,\mathrm{GHz}$, relative strength of the second carrier, $\beta = 1$, relative frequency of the second carrier , $n = 2$, and relative phase of the second carrier, $\gamma = 0$. (The blue region is susceptible to multipactor.)

diagram is shown along with the temporal relationship between the fields normal and parallel to the surface. The blue region shows the parameter regime where the multipactor discharge develops. When both components of the electric field (E_x, E_{rf}) are in this blue regime, the number of electrons N_s grows due to multipaction and the normal electric field E_x increases. Otherwise, the normal electric field E_x and hence the multipactor electron population N_s decrease. In the ac saturation state, the trajectory of (E_x, E_{rf}) is periodic and traces a closed Lissajous curve.[11] It is noteworthy that by interpolating the values of E_{rf} (y axis values) where the Lissajous curve crosses the susceptibility boundaries in Fig. 2(c) and substituting these values in the equation $E_{rf} = E_{rf0}\sin(\omega t + \theta)$, we can determine the corresponding values of time t and quantify the amount of time in a period spent by the electric fields in the growth regime (blue region of the susceptibility diagram) and in the decay regime (white region of the susceptibility diagram). For the case in Fig. 2, the time spent in the growth (decay) regime is roughly 0.2 (0.8) ns, corresponding to 20% (80%) of the rf period (1 ns).

Figures 3(a)–3(c) show the same set of plots as Figs. 2(a)–2(c) for two frequencies of the rf electric field, $E_{rf} = E_{rf0}\sin(\omega t + \theta) + \beta E_{rf0}\sin(n\omega t + \theta + \gamma)$, for the relative strength of the second carrier to the fundamental carrier, $\beta = 1$, the relative phase between the two carriers, $\gamma = 0$, and the frequency ratio of the second carrier to the fundamental carrier, $n = 2$. In contrast to Fig. 2(b), we observe an oscillation of the secondary electron yield, δ, at four times the rf frequency in Fig. 3(b). As a result, the shape of the corresponding Lissajous curve in Fig. 3(c) becomes significantly different from that of Fig. 2(c). In addition to the two large loops observed for the single frequency case, we observe two small loops in this case in the lower E_x region. This implies that the instantaneous E_x, and hence the multipactor electron population N_s, remains at a lower value for a longer duration within an rf period for dual frequency operation with the specified parameters than for single frequency operation [cf. E_x in Fig. 3(a) vs in Fig. 2(a)].

From Fig. 3(c), it is estimated that the time spent in the growth regime (blue region of the susceptibility diagram) during the small loops is 0.18 ns, whereas the time spent in the growth regime of the large loops is only 0.12 ns, which is much shorter than that of the single frequency case (0.2 ns as stated earlier). Note that though the growth time in the small loops is relatively long, the growth rate is low, resulting in a relatively small electron population during this time interval [cf. E_x in Fig. 3(a)].

Figures 4(a) and 4(b) show the multipactor susceptibility diagrams[3–5] for the rf electric field with single carrier frequency and two carrier frequencies, respectively. We observe that the slope of the lower susceptibility boundary decreases for dual frequency operation with the specified parameters, as described in Ref. 7. This suggests a higher saturation level of E_x, because multipactor saturation occurs at the lower susceptibility boundary. From the temporal study, we find that the time average value of E_x in the saturation state for the dual frequency case is $E_{x,avg,dual} \sim 1.1\,\mathrm{MV/m}$, which is higher than that for the single frequency case, $E_{x,avg,single} \sim 0.9\,\mathrm{MV/m}$. This is consistent with the susceptibility diagrams of Fig. 4. For the dual frequency case where the average power kept the same as that for the single

29 October 2024 17:02:22

Published under license by AIP Publishing

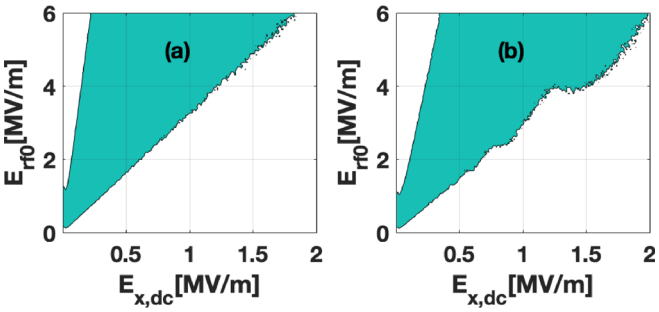

FIG. 4. Multipactor susceptibility boundaries (blue regions are subject to multipactor susceptibility) in the $(E_{x,dc}, E_{rf0})$ plane from Monte Carlo simulation: (a) with single carrier frequency of the rf field, and (b) with two carrier frequencies of the rf field (parameters specified as in Fig. 3). Here, rf frequency, $f_{rf} = 1$ GHz, the maximum secondary electron yield, $\delta_{max0} = 3$, occurring at impact energy $E_{max0} = 420$ eV, and $E_{0m}/E_{max0} = 0.005$, where $2E_{0m}$ is the average emission energy of secondary electrons. In the calculation, $E_{x,dc}$ is kept as a constant, and the susceptibility is recorded when $\delta_{avg} > 1$.

frequency case in Fig. 2 (i.e., $E_{rf0,dual} = E_{rf,rms,single} = 3/\sqrt{2}$ MV/m), the time average saturation value of the normal electric field is found to be $E_{x,avg,dual} \sim 0.75$ MV/m, which is lower than that for the single frequency case.

In summary, a temporal study was carried out on dual frequency single surface multipactor using a new MC simulation model with adaptive time steps. We found that for the dual frequency operation with a second harmonic carrier mode, the time average of normal surface field E_x and the corresponding multipactor electron population N_s are increased (for the dual-frequency case with individual carrier amplitude equal to the single carrier case), but the instantaneous E_x and N_s are reduced for a longer duration within an rf period compared to the single frequency operation.

Further studies may include temporal profiling of E_x with different parameters of the second carrier mode, space charge effects, and phase aggregation or diffusion of particles. One important improvement in our model can be the inclusion of space charge, which might bring considerable change in the numerical values of the calculations. From Gauss's law, we can conjecture that when space charge is accounted for, the particles in flight at higher altitudes will experience lower levels of the normal electric field than the particles in flight at lower altitudes; therefore, their flight times will increase. As the flight times of some particles increase, the total number of particles impacting the surface in a specific time period will decrease. However, since these particles gain more energy from the electric fields while in flight, their impact energy will be larger, giving larger secondary electron yields (provided that the impact energy is below the second crossover point in the secondary electron yield vs impact energy curve). Therefore, the effect of space charge on multipactor will be nonlinear. Understanding the extent of this effect requires further study. The inclusion of space charge would also increase the complexity and computational cost of the model.

This work was supported by AFOSR MURI Grant No. FA9550-18-1-0062 and in part by an MSU Foundation Strategic Partnership Grant.

REFERENCES

[1]P. T. Farnsworth, J. Franklin Inst. **218**, 411 (1934).
[2]J. R. M. Vaughan, IEEE Trans. Electron Devices **35**, 1172 (1988).
[3]R. A. Kishek and Y. Y. Lau, Phys. Rev. Lett. **80**, 193 (1998).
[4]R. A. Kishek, Y. Y. Lau, L. K. Ang, A. Valfells, and R. M. Gilgenbach, Phys. Plasmas **5**, 2120 (1998).
[5]P. Zhang, Y. Y. Lau, M. Franzi, and R. M. Gilgenbach, Phys. Plasmas **18**, 053508 (2011).
[6]S. Anza, M. Mattes, C. Vicente, J. Gil, D. Raboso, V. E. Boria, and B. Gimeno, Phys. Plasmas **18**, 032105 (2011).
[7]A. Iqbal, J. Verboncoeur, and P. Zhang, Phys. Plasmas **25**, 043501 (2018).
[8]S. Yamaguchi, Y. Saito, S. Anami, and S. Michizono, IEEE Trans. Nucl. Sci. **39**, 278 (1992).
[9]N. Rozario, H. F. Lenzing, K. F. Reardon, M. S. Zarro, and C. G. Baran, IEEE Trans. Microwave Theory Tech. **42**, 558 (1994).
[10]T. P. Graves, A. A. Hubble, and P. T. Partridge, "Physics-based standard for RF breakdown prevention in spacecraft components," in *Proceedings of the 2016 IEEE International Conference on Plasma Science (ICOPS)* (2016), pp. 1–1.
[11]H. C. Kim and J. P. Verboncoeur, Phys. Plasmas **12**, 123504 (2005).
[12]J. R. M. Vaughan, IEEE Trans. Electron Devices **36**, 1963 (1989).
[13]R. M. Vaughan, IEEE Trans. Electron Devices **40**, 830 (1993).
[14]A. Valfells, J. P. Verboncoeur, and Y. Y. Lau, IEEE Trans. Plasma Sci. **28**, 529 (2000).

29 October 2024 17:02:22

Published under license by AIP Publishing